Chemical Physics Letters 763 (2021) 138229

Contents lists available at ScienceDirect

Chemical Physics Letters

journal homepage: www.elsevier.com/locate/cplett

Research paper

O_2 adsorption on defective Penta-Graphene lattices: A DFT study

Kleuton A. Lopes Lima, Marcelo L. Pereira Júnior, Fábio F. Monteiro, Luiz F. Roncaratti, Luiz A. Ribeiro Júnior *

Institute of Physics, University of Brasília, 70910-900, Brasília, Brazil

HIGHLIGHTS

- The adsorption mechanism of an O_2 molecule on defective PG is revealed.
- The calculated adsorption energies pointed for good sensing properties of PG.
- The defective PG lattice can present a degree of selectivity for O_2 sensing.

GRAPHICAL ABSTRACT

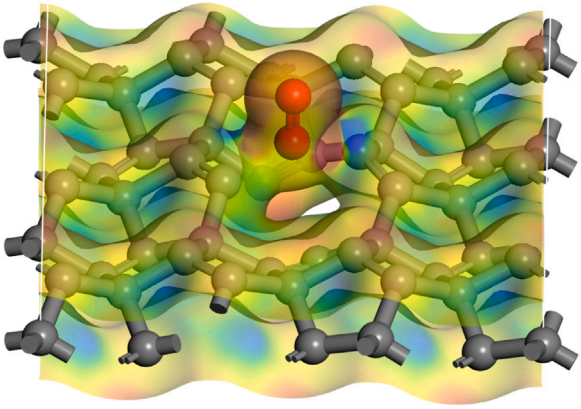

ARTICLE INFO

Keywords:
Oxygen adsorption
Penta-Graphene
Sensors
DFT
Improved Lennard-Jones

ABSTRACT

Penta-Graphene (PG) was theoretically proposed as a new carbon allotrope with a 2D structure. PG has revealed interesting gas sensing properties. Here, the structural and electronic properties of defective PG lattices interacting with an oxygen molecule were theoretically studied by employing density functional theory calculations. Results show that PG lattices with a sp^3-like single-atom vacancy presented higher adsorption energy than the sp^2-like one. Remarkably, PG lattices with a sp^3-like defect presented a clear degree of selectivity for the molecule orientation by changing their bandgap configurations. Importantly, the adsorption energies were obtained using the improved Lennard-Jones (ILJ) potential.

1. Introduction

In the last two decades, the need for environmental, industrial, and biological monitoring of O_2 concentration has stimulated the growing interest in developing new oxygen sensor technologies [1–3]. Carbon-based 3D and 2D nanomaterials are known as suitable sensors of small molecules such as O_2, CO, NO, and NO_2 with the potential of monitoring low concentrations of these gases, presenting optimal response times [4–10]. Particularly, 2D structures of these nanomaterials have been both experimentally and theoretically studied regarding their potential of acting as gas sensors, mostly due to their large surface area and high carrier mobility [11–13]. In this sense, it was reported recently that the electronic properties of 2D nanomaterials, such as graphene and MoS_2, are altered upon adsorption of small molecules [14,15].

Pristine graphene presents a stable sp^2-like hybridization of carbon bonds and null bandgap [16–18]. These features make it inefficient for gas adsorption and, therefore, not suitable for developing gas sensor devices. On the other hand, Penta-Graphene (PG) – a new 2D carbon

* Corresponding author.
E-mail address: ribeirojr@unb.br (L.A. Ribeiro Júnior).

https://doi.org/10.1016/j.cplett.2020.138229
Received 25 July 2020; Accepted 25 November 2020
Available online 28 November 2020

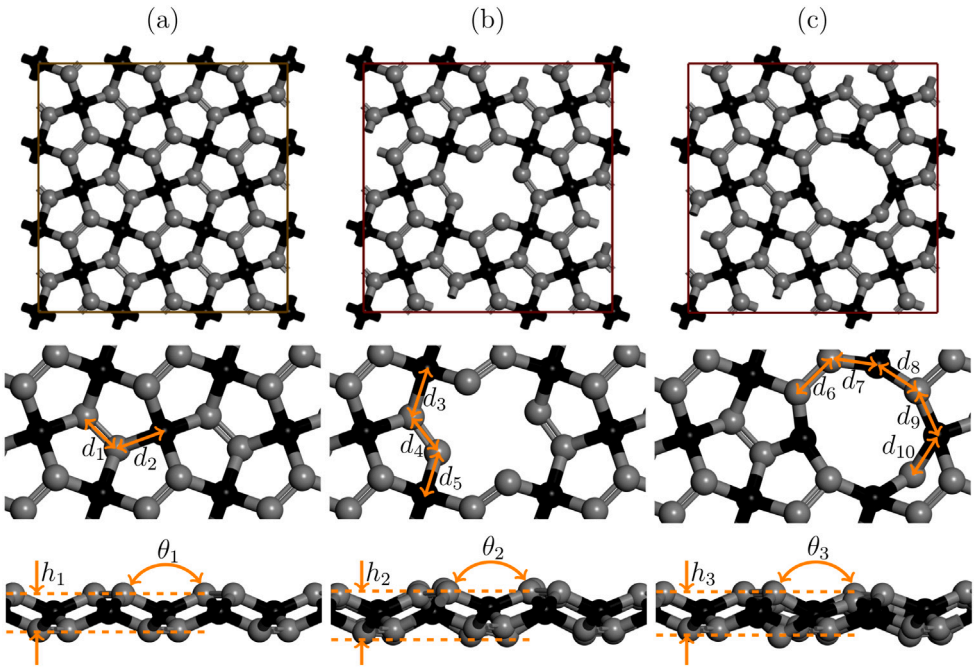

Fig. 1. Top panels: Schematic representation for the ground state configurations of (a) non-defective PG, (b) a PG lattice with monovacancy defect at a sp^3-hybridized carbon atom, and (c) a PG lattice with monovacancy defect at a sp^2-hybridized carbon atom. Middle panels: enlarged regions to highlight the lattice defects. Bottom panels: side view of the PG lattices. In the color scheme, the sp^3-hybridized carbon atoms are the black spheres and sp^2-hybridized carbon atoms are the gray ones. (For interpretation of the references to color in this figure legend, the reader is referred to the web version of this article.)

allotrope with a Cairo tessellation based lattice (pentagonal arrangement of atoms) [19,20] – was theoretically proposed as a structure that contains both sp^3-like and sp^2-like hybridizations of carbon bonds, which are more interesting when it comes to open new channels for the gas adsorption mechanism [21,22]. Due to the tetrahedral character of the sp^3-like hybridization, the PG surface is not precisely flat, which suggests the existence of regions with a higher chance for the adsorption of molecules. This particular feature also broadens the options to use PG as an active layer in novel sensor prototypes [19]. Although PG has shown promising trends to develop gas sensor applications [23], due to its unavailability of synthesis, investigations in this direction are still scarce.

Some theoretical contributions in the literature, mostly based on the density functional theory (DFT) calculations, have investigated the adsorption mechanism of small molecules in PG [23,24,24–30]. Generally, the results have revealed the existence of substantial adsorption energies for the complex molecule/PG with moderate charge transfer for small molecules such as H_2O, H_2S, NH_3, SO_2, and NO [25]. When it comes to the adsorption mechanism of oxygen molecules on PG lattices, studies in the literature are very few [26]. It is well known that the presence of lattice defects is inevitable during the manufacturing process of nanomaterials [31–33]. In this sense, investigations that take into account the impact of single-atom vacancies on the interaction between small molecules and PG membranes can contribute to gain a broader understanding of the adsorption mechanism in systems with carbon-based active layers.

Herein, we employed DFT calculations to numerically study the effect of O_2 adsorption on the electronic and structural properties of PG lattices endowed of single-atom vacancies. Remarkably, our results point to the possibility of O_2 adsorption on PG at room temperature with reasonable adsorption energy, low recovering time, and a good degree of selectivity. The calculations performed here suggest that PG can be a promising candidate for the production of O_2 sensors and open a channel for the understanding of the adsorption mechanism of small molecules in carbon-based lattices.

2. Methodology

The structural and electronic properties of PG/O_2 complexes were studied using the DMol^3 module as implemented in Biovia Materials Studio software [34–36]. In all calculations, the Local Density Approximation (LDA) is considered employing the Perdew–Wang (PWC) functional with unrestricted spin (DNP), and a numerical basis set of atomic orbitals with polarized functions [37,38]. The BSSE correction is used through the counterpoise method, and the nuclei-valence electron interactions are represented by the inclusion of semi-core DFT pseudopotentials [39]. The K points in the Brillouin zone are considered within a 14 × 14 × 1 Monkhorst–Pack mesh [40]. Ground state structures for the PG lattices, as presented in Fig. 1, are obtained by defining the following tolerances: 1×10^{-5} for the self-consistent field, 0.002 Ha/Å for maximum force, and 0.005 Å for maximum displacement. A 3 × 3 supercell with a vacuum space of 30 Å is used to model the interacting PG/O2 complexes. It is worthwhile to stress that this set of parameters was successfully used in other theoretical studies, where the adsorption of small molecules on the surface of nanostructures was also investigated [41–44].

In Fig. 1, the PG lattices contain sp^3-hybridized carbon atoms (black spheres) and sp^2-hybridized carbon atoms (gray spheres). Fig. 1(a) presents the ground state structure for a non-defective lattice (PG). Fig. 1(b) and (c) depict the ground state structures for PG lattices with a monovacancy defect at sp^3-hybridized (PG@A) and sp^2-hybridized carbon (PG@B) atoms, respectively. It is worthwhile to stress that these structures were studied very recently [27]. The structural parameters obtained here (highlighted in Fig. 1) are d (in-plane C–C distance), h (out-of-plane C–C distance), and θ (planarity degree). Their values are: d_1 = 1.34 Å, d_2 = 1.54 Å, d_3 = 1.55 rA, d_4 = 1.33 Å, d_5 = 1.50 Å, d_6 = 1.37 Å, d_7 = 1.41 Å, d_8 = 1.45 Å, d_9 = 1.51 Å, d_{10} = 1.51 Å, h_1 = 0.039 Å, h_2 = 0.050 Å, h_3 = 0.047 Å, θ_1 = 135.01°, θ_2 = 139.21°, and θ_3 = 137.63°. Importantly, these values are in good agreement with the ones reported in other theoretical studies in literature [23,27].

In our computational approach, the O_2 molecule is positioned parallel (O_2-H) or perpendicular (O_2-V) to the PG plane, at an initial

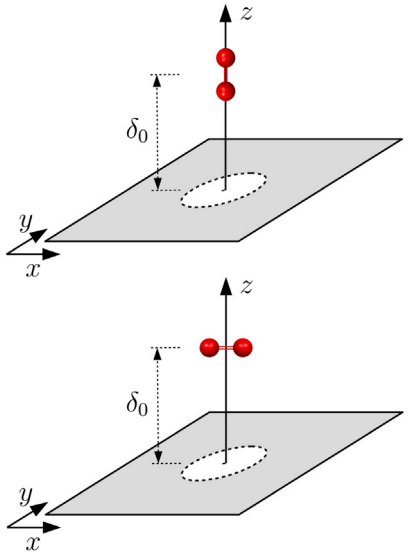

Fig. 2. Schematic representation of the computational approach (initial system configurations) used here to obtain the adsorption energy curves for the O_2 interaction with all the PG lattices presented in Fig. 1. The O_2 molecule is initially positioned 7 Å above the PG plane.

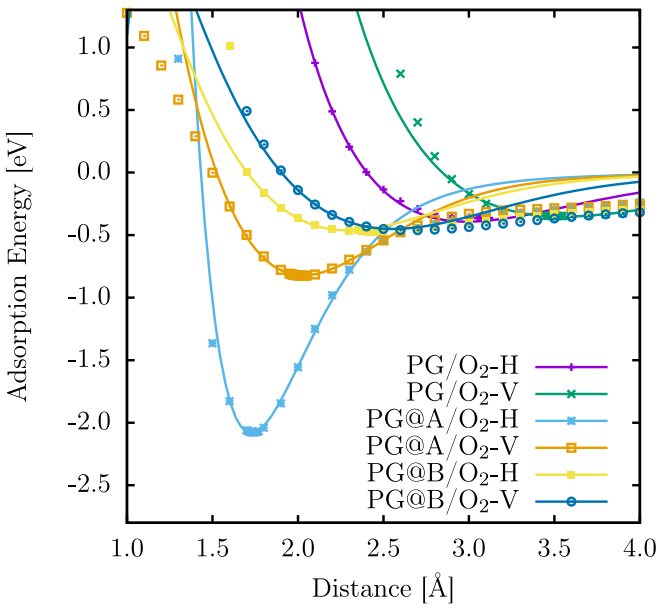

Fig. 3. Adsorption energy curves for all the PG/O_2 complexes studied here. The curves were fitted using the ILJ equation [45]. The initial configurations are illustrated in Fig. 2.

distance of 7.0 Å (see Fig. 2). The adsorption mechanism for these PG/O2 complexes was investigated considering six cases, where the O_2 molecule approaches the PG, PG@A, and PG@B surfaces, forming the following complexes: PG/O_2-H, PG/O_2-V, PG@A/O_2-H, PG@A/O_2-V, PG@B/O_2-H, and PG@B/O_2-V. In Fig. 2, δ_0 represents the distance between the centroids of the molecule and the PG lattice. By varying δ_0, the O_2 moved towards the PG plane and we obtained adsorption energy (E_{ads}) curves using the expression: $E_{ads} = E_{(PG+O_2)} - E_{PG} - E_{O_2}$, where E_{PG}, E_{O_2}, and $E_{(PG+O_2)}$ are the total energies for isolated PG, isolated O_2, and O_2 adsorbed on PG surface, respectively. For a more detailed description of the PG/O_2 adsorption mechanism, the case of higher adsorption energy is further investigated through its electronic properties. This case was identified through the adsorption energy curves. These curves were fitted using the Improved Lennard-Jones (ILJ) equation [45].

3. Results

We begin our discussions by presenting the adsorption energy curves that were obtained using the protocol discussed above. Fig. 3 displays these curves and their related ILJ fitting [45]. In this figure, one can note that the interplay between the adsorption energy and the distance between O_2 and PG yields typical potential energy curves. The PG/O_2-H, PG/O_2-V, PG@B/O_2-H, and PG@B/O_2-V showed a physisorption mechanism since their curves dot not present a clearly defined potential well. In these systems, the electronic properties of the adsorbent are slightly changed in the presence of an adsorbate (as discussed later). The obtained adsorption energies (ϵ parameter in Ref. [45]) and equilibrium distances (r_m) are presented in Table 1. These values for PG/O_2-H, PG/O_2-V, PG@B/O_2-H, and PG@B/O_2-V cases are similar to the ones obtained in other theoretical studies in which the adsorption of an oxygen molecule on pristine boron-nitrite and graphene membranes were considered [46,47]. A different adsorption mechanism is obtained for PG lattices endowed with a sp^3-type vacancy. In Fig. 3, one can note that the PG@A/O_2-H e PG@A/O_2-V cases present higher reactivity (or higher adsorption energies) than the other cases. The adsorption energy for the PG@A/O_2-H case is, at least, twice higher than all the other cases. Particularly, the adsorption process in PG@A/O_2-H system denotes a chemisorption mechanism,

Table 1
Calculated adsorption energies ϵ and equilibrium distances r_m from the curve fitting presented in Fig. 3, which was performed through the ILJ equation [45].

System	ϵ [eV]	r_m [Å]
PG/O_2-H	0.39	2.99
PG/O_2-V	0.35	3.55
PG@A/O_2-H	2.08	1.72
PG@A/O_2-V	0.82	2.03
PG@B/O_2-H	0.46	2.29
PG@B/O_2-V	−0.53	2.55

and the electronic properties of the PG are affected by its interaction with the O_2 molecule, as it will be discussed later. In contrast with the PG and PG@B cases, the PG@A/O_2-H e PG@A/O_2-V curves present a potential well. The vertical orientation of the O_2 molecule, regarding the PG plane, leads the two oxygen atoms to interact almost in the same fashion with the PG@A sheet. This trend is not observed in the PG@A/O_2-V case in which only one of the oxygen atoms is positioned close to the PG@A surface. Moreover, in the PG@A lattice, the atoms within the defective region are closer to each other than in the PG@B one. This feature is due to a tendency of the carbon atoms in forming new bonds in the vicinity of the vacancy, which reduces the area of the defective region and increases the electrostatic potential.

To obtain an extended description of the adsorption energies of the O_2/PG complexes studied here, we show in Fig. 4 the adsorption energy maps for the minimum energy configurations in the PG@A/O_2-V (Fig. 4(a)) and PG@A/O_2-H (Fig. 4(b)) cases. These maps were obtained by varying the position of the O_2 molecule (with a step of 0.5 Å) in the x and y directions of the PG surface. The main conclusions hold and the depth well of the O_2/PG interactions are still the same shown in the potential energy curves (see Fig. 3). The O_2/PG interaction energies in the regions without a lattice defect are considerably lower than the ones within/nearby the vacancy.

Now, we analyze the recovering time (τ) [48] – that corresponds to the transient time in which the molecule adsorption takes place – for the systems with better adsorption performances (PG@A/O_2-H e PG@A/O_2-V). The recovering time is calculated as $\tau = 1\nu \times exp(-E_{ads}/k_BT)$, where ν is the molecule oscillation frequency (10^{12} s^{-1} [49]), k_B is the Boltzmann constant, and T the temperature (298 K).

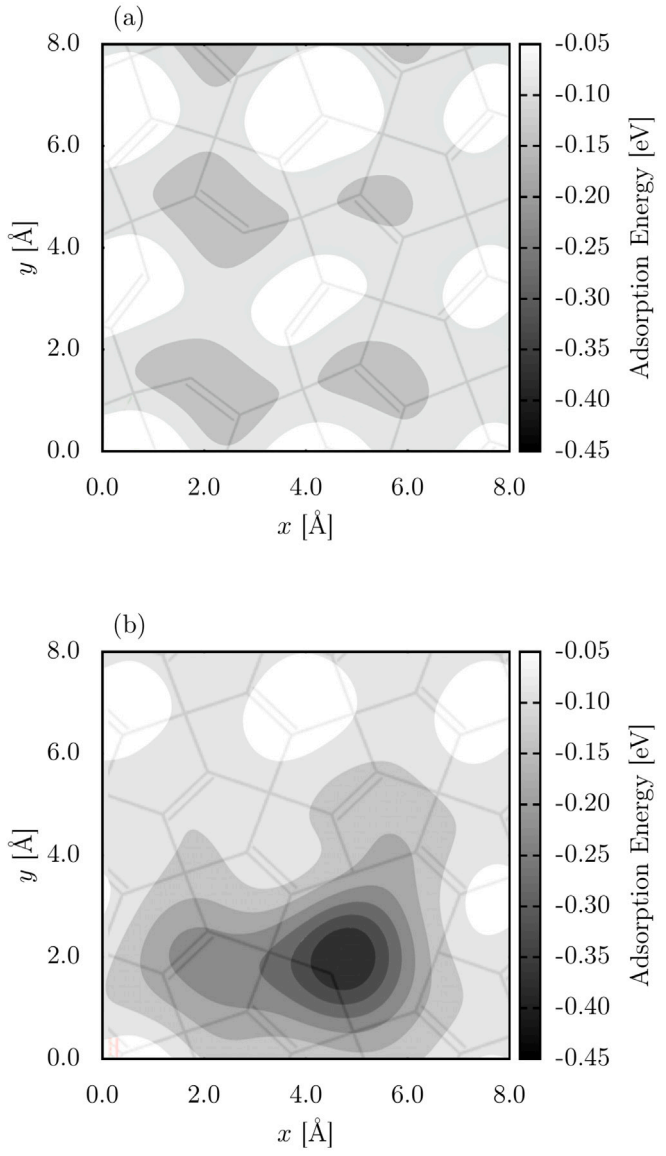

Fig. 4. Adsorption energy maps for the minimum energy configurations in the (a) PG@A/O_2-H and (b) PG@A/O_2-V cases.

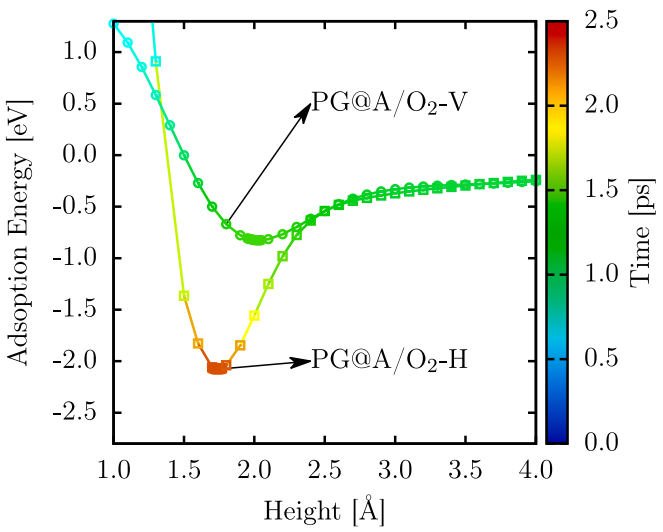

Fig. 5. Recovering time values for PG@A/O_2-H and PG@A/O_2-V adsorption energy curves, depicted in Fig. 3. The recovering time values are presented in the color palette. (For interpretation of the references to color in this figure legend, the reader is referred to the web version of this article.)

In Fig. 5, the recovering time values for PG@A/O_2-H and PG@A/O_2-V adsorption energy curves are presented in the color palette. In this way, one can note that the recovering time varies from 0.5 ps up to 2.5 ps. For the lowest absorption energy (PG@A/O_2-H case) $\tau = 2.31$ ps whereas for the PG@A/O_2-V one, the highest recovering time is about 1.5 ps. It is worthwhile to stress that the transient times obtained for the O_2 adsorption in the PG@A lattice are large enough to realize the interaction between them, which changes the electronic properties of the PG (as discussed below), before the molecule diffusion.

The electronic band structures for the systems investigated here are presented in Fig. 6. The left-most panel illustrates that the non-defective PG presents a quasi-direct bandgap of about 2.35 eV, which is in good agreement with the values reported in the Refs. [19,23,30]. As expected, the inclusion of a single-atom vacancy leads to the appearance of energy levels within the bandgap. Similar band structure signatures for the PG@A and PG@B cases were reported in other DFT-based studies [30]. Upon adsorption, the valence and conduction bands of non-defective PG suffer an energy shifting (about −1.1 eV) for the PG/O_2-H and PG/O_2-V cases, preserving the initial PG bandgap value, and a flat midgap level (the O_2 energy level) appears nearby the Fermi level. These small changes in the bandgap configuration for the non-defective PG/O_2-H and PG/O_2-V systems, and their related low values of absorption energy, denote that this kind of PG lattice is not a useful nanostructure when it comes to gas sensing applications. This trend was also reported for the graphene case [46,47]. The four right-most panels (PG@A/O_2-H, PG@A/O_2-V, PG@B/O_2-H, PG@B/O_2-V) show that electronic band structure of defective PG lattices upon O_2 adsorption are substantially impacted. As discussed above, these cases have presented higher adsorption energies. Their bandgap configurations show the following common trend: upon adsorption, the bandgap value is slightly decreased and some flat midgap levels are formed. The PG@B/O_2 band structures are insensitive to the O_2 orientation regarding the PG plane whereas the PG@A/O_2 ones show changes in their configuration (i.e., PG@A lattice present a degree of selectivity).

Finally, we analyze the electrostatic potential over the structure as well as the Highest Occupied Molecular Orbital (HOMO) and Lowest Unoccupied Molecular Orbital (LUMO) configurations only for the of better adsorption performance (PG@A/O_2). The top and bottom panels of Fig. 7 illustrate, respectively, the HOMO and LUMO orbitals and the electronic potential. The PG@A/O_2-H shows the better reactivity among all the systems, once the O_2 molecule has a considerable degree of electronegativity while the PG@A lattice presents an excess of non-bonding electrons in the vicinity of the vacancy (sp^3-like single-atom vacancy). This feature is illustrated by the electrostatic potential results, as shown in the bottom panels of Fig. 7. The HOMO (green spots) and LUMO (pink spots) changed their localization upon the O_2 adsorption, as can be seen in the top panels of Fig. 7. Notably, in the PG@A/O_2-H, part of the O_2 HOMO/LUMO orbital is delocalized on the PG surface. In this delocalization pattern, overlapping between the O_2 and PG@A orbitals takes place, which considerably enhances the interaction between. This orbitals overlapping is the main responsible in promoting the higher adsorption energy values and, consequently, the higher recovering time and changes in the electronic band structure discussed above (Figs. 5 and 6, respectively). It is worthwhile to stress that in the PG@B cases (sp^2-like single-atom vacancy) the bond reconstructions (see Fig. 1) substantially diminishes the number of non-bonding electrons in the vicinity of the vacancy. Due to this reason, the PG@B cases presented lower adsorption energies when contrasted to the PG@A ones.

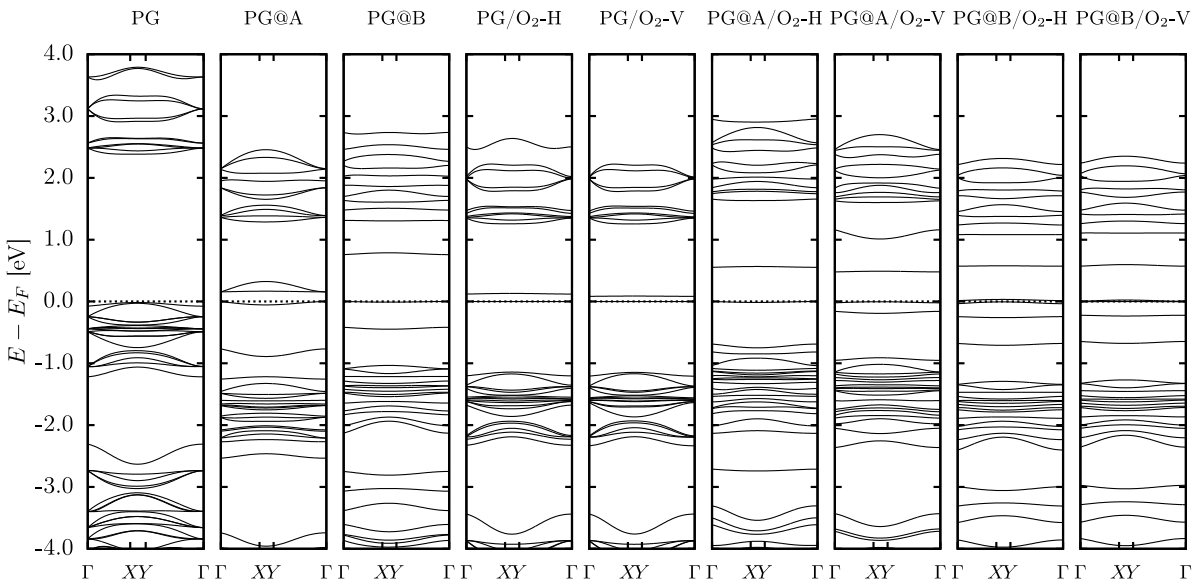

Fig. 6. Electronic band structures for the systems investigated.

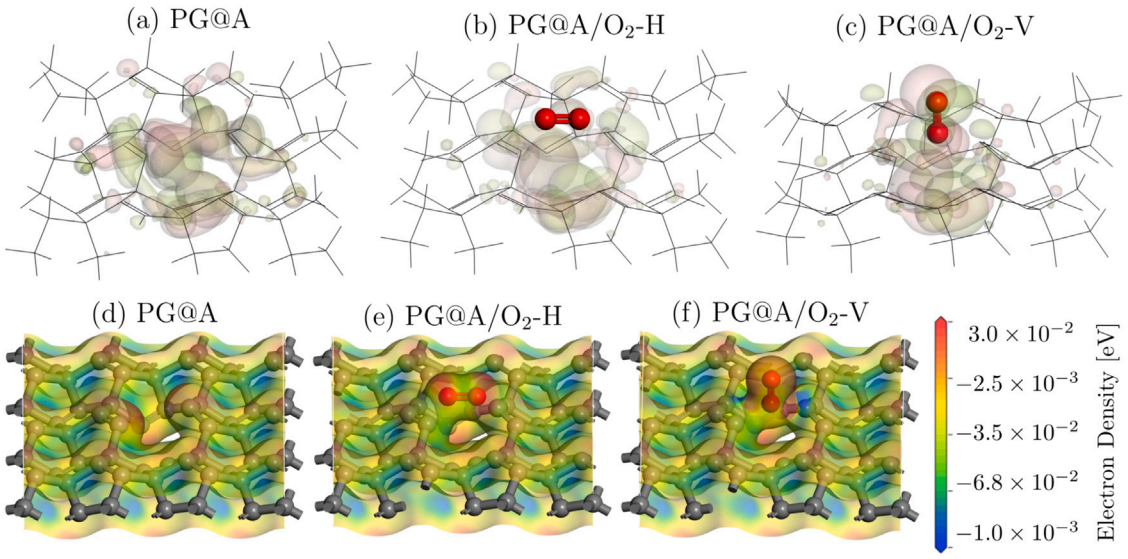

Fig. 7. (top panels) Electrostatic potential over the structure and (bottom panels) the Highest Occupied Molecular Orbital (HOMO) and Lowest Unoccupied Molecular Orbital (LUMO) configurations for the case of higher adsorption energy (PG@A/O_2). In the color scheme for the top panels, the HOMO and LUMO orbitals are represented by the green and pink spots, respectively. (For interpretation of the references to color in this figure legend, the reader is referred to the web version of this article.)

4. Conclusions

In summary, we carried out DFT calculations to investigate the O_2 adsorption mechanism on the surface of PG lattices endowed of single-atom vacancies. In our computational approach, the O_2 molecule is positioned parallel (O_2-H) or perpendicular (O_2-V) to the PG plane, at an initial distance of 7.0 Å. The adsorption mechanism for these PG/O2 complexes was investigated considering six cases, where the O_2 molecule approaches the PG, PG@A (defect created by removing a carbon atom with sp^2 hybridization), and PG@B (defect created by removing a carbon atom with sp^3 hybridization) surfaces, forming the following complexes: PG/O_2-H, PG/O_2-V, PG@A/O_2-H, PG@A/O_2-V, PG@B/O_2-H, and PG@B/O_2-V. For a more detailed description of the PG/O_2 adsorption mechanism, the case of higher adsorption energy is further investigated through its electronic properties. This case was identified through the adsorption energy curves and maps. The curves were fitted using the Improved Lennard-Jones (ILJ) equation [45].

By employing the computational protocol discussed above, our results have revealed that the relationship between the adsorption energy and the distance between O_2 and PG yields typical potential energy curves. The PG/O_2-H, PG/O_2-V, PG@B/O_2-H, and PG@B/O_2-V showed a physisorption mechanism. On the other hand, the PG@A/O_2-H e PG@A/O_2-V cases present higher reactivity. The adsorption energy for the PG@A/O_2-H case is, at least, twice higher than all the other cases. Particularly, the adsorption process in PG@A/O_2-H system stands for a chemisorption mechanism. The recovering time values for PG@A/O_2-H and PG@A/O_2-V adsorption energy curves varied from 0.5 ps up to 2.5 ps. For the lowest absorption energy (PG@A/O_2-H case) τ = 2.31 ps whereas for the PG@A/O_2-V one, the highest recovering time is about 1.5 ps. These transient times were large enough to realize the interaction between O_2 and PG@A and they have allowed changes in the electronic properties of the PG@A lattice. The electronic band structure of defective PG lattices upon O_2 adsorption is substantially impacted. Their bandgap configurations show the following common trend: upon adsorption, the bandgap value is slightly decreased and

some flat midgap levels are formed. The PG@B/O_2 band structures are insensitive to the O_2 orientation regarding the PG plane whereas the PG@A/O_2 ones show changes in their configuration, by presenting a degree of selectivity.

In the PG@A/O_2-H, part of the O_2 HOMO/LUMO orbital is delocalized on the PG surface and overlapping between the O_2 and PG@A orbitals is observed, which considerably enhances the interaction between. This overlapping trend is the main responsible in promoting the higher adsorption energy values and, consequently, the higher recovering time and changes in the electronic band structure for the PG@A/O_2-H case.

We consider as a limitation of our approach the low number of O_2 orientations concerning the PG surface. For sure, a larger number of these orientations can better describe the adsorption energy surfaces for the O_2/PG complexes. We restricted our simulations to the cases presented above to reduce their computational cost, which can increase substantially when more degrees of freedom for the molecule orientation are allowed. The O_2 atmosphere forces the fast degradation (oxidation) of the nanostructure, which makes it difficult for the analysis and the comparison of the PG electronic structure before and after the O_2 adsorption. Moreover, an increase in the number of O_2 molecules also leads to an increasing in the computational cost to conclude the simulations. The nanostructure has periodic boundary conditions. In this way, the dimensions of the nanostructure are not a problem. Some theoretical studies in the literature showed that the presence of substitutional doping sites can enhance the sensing properties of carbon-based nanostructures [29,30]. The shapes of the graphene allotrope membranes are related to the sp^2 or sp^3-like hybridization of carbon atoms. Our results suggested that hybridization is an important issue that should be considered to design carbon-based nanostructured sensors.

CRediT authorship contribution statement

Kleuton A. Lopes Lima: Data curation, Formal analysis, Methodology, Writing - original draft. **Marcelo L. Pereira Júnior:** Data curation, Formal analysis, Methodology, Writing - original draft. **Fábio F. Monteiro:** Data curation, Formal analysis, Methodology, Writing - original draft. **Luiz F. Roncaratti:** Conceptualization, Supervision, Funding acquisition, Writing - review & editing. **Luiz A. Ribeiro Júnior:** Conceptualization, Supervision, Funding acquisition, Writing - review & editing.

Declaration of competing interest

The authors declare that they have no known competing financial interests or personal relationships that could have appeared to influence the work reported in this paper.

Acknowledgments

The authors gratefully acknowledge the financial support from Brazilian Research Councils CNPq, CAPES, and FAPDF and CENAPAD-SP for providing the computational facilities. L.A.R.J. gratefully acknowledges, respectively, the financial support from FAP-DF, Brazil and CNPq grants 00193.0000248/2019-32 and 302236/2018-0. L.A.R.J. gratefully acknowledges the financial support from DPI/DIRPE/UnB, Brazil (Edital DPI/DPG 03/2020) grant 23106.057541/2020-89 and from IFD/UnB, Brazil (Edital 01/2020) grant 23106.090790/2020-86.

References

[1] Daniel S. Tyson, Jason Bialecki, Felix N. Castellano, Ruthenium (II) complex with a notably longexcited state lifetime, Chem. Commun. 1 (23) (2000) 2355–2356.
[2] Gongming Wang, Yichuan Ling, Yat Li, Oxygen-deficient metal oxide nanostructures for photoelectrochemical water oxidation and other applications, Nanoscale 4 (21) (2012) 6682–6691.
[3] Marc-Antoine Stoeckel, Marco Gobbi, Sara Bonacchi, Fabiola Liscio, Laura Ferlauto, Emanuele Orgiu, Paolo Samorì, Reversible, fast, and wide-range oxygen sensor based on nanostructured organometal halide perovskite, Adv. Mater. 29 (38) (2017) 1702469.
[4] O. Leenaerts, B. Partoens, F.M. Peeters, Adsorption of h_2o, NH_3, CO, NO_2, and NO on graphene: A first-principles study, Phys. Rev. B 77 (12) (2008) 125416.
[5] Fredrik Schedin, Andrei Konstantinovich Geim, Sergei Vladimirovich Morozov, EW Hill, Peter Blake, MI Katsnelson, Kostya Sergeevich Novoselov, Detection of individual gas molecules adsorbed on graphene, Nat. Mater. 6 (9) (2007) 652–655.
[6] Wei Hu, Nan Xia, Xiaojun Wu, Zhenyu Li, Jinlong Yang, Silicene as a highly sensitive molecule sensor for NH_3, NO and NO_2, Phys. Chem. Chem. Phys. 16 (15) (2014) 6957–6962.
[7] Wenjing Yuan, Anran Liu, Liang Huang, Chun Li, Gaoquan Shi, High-performance NO_2 sensors based on chemically modified graphene, Adv. Mater. 25 (5) (2013) 766–771.
[8] Lu Bai, Zhen Zhou, Computational study of B-or N-doped single-walled carbon nanotubes as NH_3 and NO_2 sensors, Carbon 45 (10) (2007) 2105–2110.
[9] yacheslav O. Khavrus, Hartmut Vinzelberg, Joachim Schumann, Albrecht Leonhardt, Steffen Oswald, Bernd Büchner, On the potential of long carbon nanotube forest for sensing gases and vapors, Phys. E 43 (6) (2011) 1199–1207.
[10] Hubert Valencia, Adrià Gil, Gilles Frapper, Trends in the adsorption of 3d transition metal atoms onto graphene and nanotube surfaces: A DFT study and molecular orbital analysis, J. Phys. Chem. C 114 (33) (2010) 14141–14153.
[11] Xianping Chen, Cell K.Y. Wong, Cadmus A. Yuan, Guoqi Zhang, Nanowire-based gas sensors, Sensors Actuators B 177 (2013) 178–195.
[12] Zhen Zhu, David Tománek, Semiconducting layered blue phosphorus: a computational study, Phys. Rev. Lett. 112 (17) (2014) 176802.
[13] Rui-Shen Meng, Miao Cai, Jun-Ke Jiang, Qiu-Hua Liang, Xiang Sun, Qun Yang, Chun-Jian Tan, Xian-Ping Chen, First principles investigation of small molecules adsorption on antimonene, IEEE Electron Device Lett. 38 (1) (2016) 134–137.
[14] Byungjin Cho, Myung Gwan Hahm, Minseok Choi, Jongwon Yoon, Ah Ra Kim, Young-Joo Lee, Sung-Gyu Park, Jung-Dae Kwon, Chang Su Kim, Myungkwan Song, et al., Charge-transfer-based gas sensing using atomic-layer mos_2, Sci. Rep. 5 (2015) 8052.
[15] Jian Zhen Ou, Wanyin Ge, Benjamin Carey, Torben Daeneke, Asaf Rotbart, Wei Shan, Yichao Wang, Zhengqian Fu, Adam F Chrimes, Wojtek Wlodarski, et al., Physisorption-based charge transfer in two-dimensional sns_2 for selective and reversible NO_2 gas sensing, ACS Nano 9 (10) (2015) 10313–10323.
[16] P Blake, EW Hill, AH Castro Neto, KS Novoselov, D Jiang, R Yang, TJ Booth, AK Geim, Making graphene visible, Appl. Phys. Lett. 91 (6) (2007) 063124.
[17] Rahul Raveendran Nair, Peter Blake, Alexander N Grigorenko, Konstantin S Novoselov, Tim J Booth, Tobias Stauber, Nuno MR Peres, Andre K Geim, Fine structure constant defines visual transparency of graphene, Science 320 (5881) (2008) 1308.
[18] AH Castro Neto, Francisco Guinea, Nuno MR Peres, Kostya S Novoselov, Andre K Geim, The electronic properties of graphene, Rev. Modern Phys. 81 (1) (2009) 109.
[19] Zhang Shunhong, Zhou Jian, Wang Qian, Chen Xiaoshuang, Kawazoe Yoshiyuki, Jena Puru, Penta-graphene: A new carbon allotrope, Radio Electron. Nanosyst. Inform. Technology. 7 (2) (2015).
[20] Christopher P. Ewels, Xavier Rocquefelte, Harold W. Kroto, Mark J. Rayson, Patrick R. Briddon, Malcolm I. Heggie, Predicting experimentally stable allotropes: Instability of penta-graphene, Proc. Natl. Acad. Sci. 112 (51) (2015) 15609–15612.
[21] E.M. Stuve, R.J. Madix, Use of the .pi..sigma. parameter for characterization of rehybridization upon adsorption on metal surfaces, J. Phys. Chem. 89 (15) (1985) 3183–3185.
[22] FL Coffman, R Cao, PA Pianetta, S Kapoor, M Kelly, LJ Terminello, Near-edge x-ray absorption of carbon materials for determining bond hybridization in mixed sp_2/sp_3 bonded materials, Appl. Phys. Lett. 69 (4) (1996) 568–570.
[23] Hongbo Qin, Chuang Feng, Xinghe Luan, Daoguo Yang, First-principles investigation of adsorption behaviors of small molecules on penta-graphene, Nanoscale Res. Lett. 13 (1) (2018) 1–7.
[24] Dachang Chen, Xiaoxing Zhang, Ju Tang, Hao Cui, Zhenwei Chen, Yi Li, Different doping of penta-graphene as adsorbent and gas sensing material for scavenging and detecting SF_6 decomposed species, Sustainable Materials and Technologies 21 (2019) e00100.
[25] Meng-Qi Cheng, Qing Chen, Ke Yang, Wei-Qing Huang, Wang-Yu Hu, Gui-Fang Huang, Penta-graphene as a potential gas sensor for NO_x detection, Nanoscale Res. Lett. 14 (1) (2019) 306.

[26] Lin Li, Kaixuan Jin, Chunyan Du, Xiaojie Liu, The effect of oxidation on the electronic properties of penta-graphene: first-principles calculation, RSC Adv. 9 (15) (2019) 8253–8261.
[27] Aaditya Manjanath, Chao-Ping Hsu, Yoshiyuki Kawazoe, Tuning the electronic and magnetic properties of pentagraphene through the c_1 vacancy, 2D Mater. (2020).
[28] Tran Yen Mi, Dang Minh Triet, Nguyen Thanh Tien, Adsorption of gas molecules on penta-graphene nanoribbon and its implication for nanoscale gas sensor, Phys. Open 2 (2020) 100014.
[29] C. Feng, X. Luan, P. Zhang, J. Xiao, D. Yang, H. Qin, A first-principle study of the adsorption behavior of NO gas molecules on pristine and al-doped penta-graphene, in: 2017 18th International Conference on Electronic Packaging Technology (ICEPT), 2017, pp. 1138–1142.
[30] John Isaac G. Enriquez, Al Rey C. Villagracia, Hydrogen adsorption on pristine, defected, and 3d-block transition metal-doped penta-graphene, Int. J. Hydrogen Energy 41 (28) (2016) 12157–12166.
[31] Landong Li, Junqing Yan, Tuo Wang, Zhi-Jian Zhao, Jian Zhang, Jinlong Gong, Naijia Guan, Sub-10 nm rutile titanium dioxide nanoparticles for efficient visible-light-driven photocatalytic hydrogen production, Nat. Commun. 6 (1) (2015) 1–10.
[32] Jaison Jeevanandam, Ahmed Barhoum, Yen S Chan, Alain Dufresne, Michael K Danquah, Review on nanoparticles and nanostructured materials: history, sources, toxicity and regulations, Beilstein J. Nanotechnol. 9 (1) (2018) 1050–1074.
[33] Imali A. Mudunkotuwa, Vicki H. Grassian, The devil is in the details (or the surface): impact of surface structure and surface energetics on understanding the behavior of nanomaterials in the environment, J. Environ. Monit. 13 (5) (2011) 1135–1144.
[34] B. Delley, An all-electron numerical method for solving the local density functional for polyatomic molecules, J. Chem. Phys. 92 (1) (1990) 508–517.
[35] B. Delley, From molecules to solids with the $dmol_3$ approach, J. Chem. Phys. 113 (18) (2000) 7756–7764.
[36] Jan Andzelm, Christoph Kölmel, Andreas Klamt, Incorporation of solvent effects into density functional calculations of molecular energies and geometries, J. Chem. Phys. 103 (21) (1995) 9312–9320.
[37] John P. Perdew, Yue Wang, Accurate and simple analytic representation of the electron-gas correlation energy, Phys. Rev. B 45 (23) (1992) 13244.
[38] Walter Kohn, Lu Jeu Sham, Self-consistent equations including exchange and correlation effects, Phys. Rev. 140 (4A) (1965) A1133.
[39] B. Delley, Hardness conserving semilocal pseudopotentials, Phys. Rev. B 66 (2002) 155125.
[40] Hendrik J. Monkhorst, James D. Pack, Special points for brillouin-zone integrations, Phys. Rev. B 13 (1976) 5188–5192.
[41] Kleuton Antunes Lopes Lima, Wiliam Ferreira da Cunha, Fábio Ferreira Monteiro, Marcelo Lopes Pereira Jr, Luiz Antonio Ribeiro Jr, Adsorption of carbon dioxide and ammonia in transition metal–doped boron nitride nanotubes, J. Mol. Model. 25 (2019).
[42] Edson Nunes Costa Paura, Wiliam F. da Cunha, Pedro H. de Oliveira Neto, Geraldo M. e Silva, Joao B.L. Martins, Ricardo Gargano, Vibrational and electronic structure analysis of a carbon dioxide interaction with functionalized single-walled carbon nanotubes, J. Phys. Chem. A 117 (13) (2013) 2854–2861, PMID: 23425025.
[43] Edson N.C. Paura, Wiliam F. da Cunha, João Batista Lopes Martins, Geraldo Magela e Silva, Luiz F. Roncaratti, Ricardo Gargano, Carbon dioxide adsorption on doped boron nitride nanotubes, RSC Adv. 4 (2014) 28249–28258.
[44] Igo T. Lima, Ricardo Gargano, Silvete Guerini, Edson N.C. Paura, A theoretical study of adsorbed non-metallic atoms on magnesium chloride monolayers, New J. Chem. 43 (2019) 7778–7783.
[45] Fernando Pirani, Simona Brizi, Luiz F. Roncaratti, Piergiorgio Casavecchia, David Cappelletti, Franco Vecchiocattivi, Yond the lennard-jones model: a simple and accurate potential function probed by high resolution scattering data useful for molecular dynamics simulations, Phys. Chem. Chem. Phys. 10 (2008) 5489–5503.
[46] H.J. Yan, B. Xu, S.Q. Shi, C.Y. Ouyang, First-principles study of the oxygen adsorption and dissociation on graphene and nitrogen doped graphene for li-air batteries, J. Appl. Phys. 112 (10) (2012) 104316.
[47] Qiao Sun, Caixia Sun, Aijun Du, Shixue Dou, Zhen Li, In-plane graphene/boron-nitride heterostructures as an efficient metal-free electrocatalyst for the oxygen reduction reaction, Nanoscale 8 (2016) 14084–14091.
[48] Kriengkri Timsorn, Chatchawal Wongchoosuk, Adsorption of NO2, HCN, HCHO and CO on pristine and amine functionalized boron nitride nanotubes by self-consistent charge density functional tight-binding method, Mater. Res. Express 7 (5) (2020) 055005.
[49] Shu Peng, Kyeongjae Cho, Pengfei Qi, Hongjie Dai, Ab initio study of CNT NO_2 gas sensor, Chem. Phys. Lett. 387 (4) (2004) 271–276.